J. Water Environ. Nanotechnol., 7(1): 101-120 Winter 2022

ORIGINAL RESEARCH PAPER

Effect of pH on Green Synthesis of Reduced Graphene Oxide Using Lemon Extract and Application of Fe_3O_4/RGO nanocomposites for the removal of Pb (II) from aqueous solution

Maryam Ghasemi[1*], Javad Azimi-Amin[2]

[1] Young Researchers and Elite Club, Arak Branch, Islamic Azad University, Arak, Iran
[2] Young Researchers and Elite Club, Hamedan Branch, Islamic Azad University, Hamedan, Iran

Received: 2021-10-02 Accepted: 2021-11-26 Published: 2022-02-01

ABSTRACT

Here, graphene oxide was synthesized and reduced by lemon extract (source of vitamin C) in an aqueous solution under different pH (3 and 10). The lemon extract was prepared using a solvent-free method. The proposed mechanisms for the reduction of GO may be due to the nucleophilic attack of oxygen anion of ascorbic acid to the epoxy or hydroxyl groups of GO sheets. Based on Raman spectra, with increasing the solution pH, the repair of the graphitic sp^2 domain of the RGOs decreased. Reduced graphene oxide was successfully used to synthesize Fe_3O_4/RGO nanocomposite and remove Pb ions from aqueous media. The obtained Fe_3O_4/RGO nanocomposite was characterized by XRD, FTIR, SEM, and BET analysis. Based on these characterization techniques, reduced graphene oxide is distinguishably coated by Fe_3O_4 nanoparticles. The effect of different parameters: contact time (1-60 min), initial lead concentration (25-200 mg/L), adsorbent dosage (0.01-0.07 g), and the solution's initial pH (1-8) on the removal of lead ions was studied using batch-scale tests. The maximum lead ion removal was achieved up to 90 % for Pb ions, respectively at optimum operating conditions viz. pH 5, Pb initial concentration 100 mg/L, Fe_3O_4/RGO dose 0.05 g, and contact time 30 min. Obtained results showed that the maximum adsorption capacity of Fe_3O_4/RGO for lead ion was 107.52 mg/g within 60 min of contact time. The adsorption behavior can be well described with the Langmuir isotherm and the pseudo-second-order models, indicating that the adsorption process was a monolayer and chemisorption adsorption.

Keywords: *Adsorption, Fe_3O_4 nanoparticles, Green reduction, Lemon extract, Reduced graphene oxide*

How to cite this article
Ghasemi M, Azimi-Amin J. Effect of pH on Green Synthesis of Reduced Graphene Oxide Using Lemon Extract and Application of Fe_3O_4/RGO nanocomposites for the removal of Pb (II) from aqueous solution. J. Water Environ. Nanotechnol., 2022; 7(1): 101-120. DOI: 10.22090/jwent.2022.01.008

INTRODUCTION

Heavy metals (with atomic weights between 63.5 and 200.6) are one category of toxic and non-degradable pollutants. These pollutants are found in surface- and groundwater due to the release of wastewater and effluent into them from various activities, such as industries, mining, and agriculture. The presence of these heavy metals above a certain concentration threshold leads to many disorders in the normal functioning of human beings and animals. Chromium, cadmium, copper, mercury, lead, zinc, and nickel are the most remarkable toxic compounds in effluents and wastewater [1-3]. Lead as the most toxic and long-term heavy metal is found in different industries. These industries include battery and glass manufacturing, metal plating, and the finishing or printing industry. The presence of this ion in the body leads to damage to the central nervous system, liver, kidney, and reproductive system. The symptoms of metal poisoning include anemia, insomnia, headache, dizziness, irritability, weakness of muscles, hallucinations, and renal damage. According to the US Environmental Protection

* Corresponding Author Email: *Maryam_ghasemi6282@yahoo.com, m.gh6282@gmail.com*

Agency, the maximum acceptable concentration of Pb ion in drinking water is 0.1–0.05 mg/L [4-6].

Various techniques have been used for pollutant removal from wastewater, such as coagulation, ion exchange, flocculation, membrane separation process, aerobic and anaerobic microbial degradation, adsorption, photocatalysis, and photo-oxidation [7-10]. Some of the mentioned techniques have disadvantages and often involve producing toxic sludge that is difficult to dispose of. The adsorption technique is known as one of the best for the adsorption of pollutants from wastewater, owing to its simplicity and cost-effectiveness [11]. In recent decades, researchers have used many different types of adsorbents, such as single and multi-walled carbon nanotubes, nanoparticles, nanocomposites, and low-cost adsorbents [5, 12-16].

Recently, graphene oxide (GO) and reduced graphene oxide (RGO) have been reported as efficient adsorbents for the adsorption of pollutants. These adsorbents can form complexes with metal ions as they have epoxy (–O–), hydroxyl (–OH), and carboxyl (–COOH) functional groups [17, 18]. Graphene oxide is known as a two-dimensional carbon material, and its thickness is a single atom. This material has unique electrical, optical and structural properties. These properties lead to the adsorption of molecules onto both sides of each GO sheet. Due to the large specific surface and low density of GO, this material has a high sorption capacity. Besides, graphene oxide has rich oxygen-containing groups and can be reduced by various methods, including reducing agents, and these methods can recover or repair the conjugated graphitic network [19, 20]. The dispersion of metal or metal oxides nanoparticles (NPs) onto the surface or between reduced graphene oxide sheets is an effective solution due to their functional properties [21]. A solution chemistry approach or utilizing the electrochemical deposition of metal oxide NPs onto GO sheets using microwave and ultrasound irradiation is the most widely used technique to produce metal NPs-RGO nanocomposites [22].

Ultrasonic irradiations help form the homogenization of GO solution, reduce the size of nanoparticles, and activate them in the final products [23].

The main factor is finding an appropriate reducing agent that can be used to synthesize RGO. Hydrazine (N_2H_4) [24], sodium borohydride ($NaBH_4$) [25], lithium aluminum hydride ($LiAlH_4$) [26] and hydroquinone [$C_6H_4(OH)_2$] [27] are chemical reducing agents that have been used in RGO preparation and are highly toxic, dangerous, and expensive. So, it is desirable to consider new green and natural reducing agents for the effective reduction of GO sheets. Vitamin C (Ascorbic acid) is known as an applicable and green reducing agent. Moreover, based on recent research, vitamin C is an ideal choice for the chemical reduction of GO (instead of hydrazine) [28, 29]. Lemon and lemon juice are known to be among the most notable sources of citrus vitamin C; lemon peel has the highest concentration of vitamin C; and, the obtained extract has both stabilizing and reducing features [30]. The pH values of the solution can play a crucial role in the morphology and structure of RGO samples. According to Navarro et al., the RGO that is prepared under acidic conditions has a higher amount of defects with smaller sizes of the sheets [31]. Bai et al. illustrated that the reduction process of GO under acidic conditions leads to maximum specific capacitance and an increase in the number of layers [32]. To the best of our knowledge, no studies are available on the effect of pH on the green synthesis of RGO.

The purpose of this research is to investigate the effect of pH on the green reduction of RGO using lemon extract, natural and green reducing agent, as the reducing and capping agent and synthesis of Fe_3O_4/RGO nanocomposite. This nanocomposite consisting of magnetic nanoparticles can be easily separated from the solution with the external magnet. It is the first report on the synthesis of RGO using the lemon extract prepared based on a solvent-free method. The novel nanocomposite was characterized by XRD, FTIR, SEM, and BET analysis. Lead (Pb) ion was selected as a model pollutant to investigate the adsorption process in batch-scale tests.

MATERIALS AND METHODS

Materials

The chemicals and reagents used in this study were graphite powder, sulphuric acid (98%) (H_2SO_4), nitric acid (67–70%) (HNO_3), iron chloride hexahydrate ($FeCl_3.6H_2O$), potassium permanganate ($KMnO_4$), sodium nitrate ($NaNO_3$), hydrogen peroxide (30%) (H_2O_2), sodium sulfite (Na_2SO_4), lead (II) nitrate hexahydrate ($Pb(NO_3)_2.6H_2O$), sodium hydroxide (NaOH), and hydrochloric acid (HCl), that were acquired from Merck and Sigma–Aldrich. Fresh lemons were

purchased from a local market in Hamadan, Iran.

Preparation of lemon extract

The lemons were washed in double-deionized water, then 500 g of washed and dried lemons were put in a closed-door flask in the sunshine. After ten days, the obtained extract was filtered using Whatman filter paper then stored in a refrigerator.

Preparation of GO and RGO

Graphene oxide (GO) was prepared using the improved Hummer method [33]. In summary, as the first step, a mixture of 3 g of graphite and 1 g of $NaNO_3$ were stirred in 46 mL of H_2SO_4 in an ice-water bath for 30 min. As the second step, 6 g of $KMnO_4$ was slowly added to the above mixture. The mixture was stirred continuously for two h in an ice-water bath and then at 35 ℃ for 24 h. As the third step, 138 mL of deionized water was slowly added to the mixture, and its temperature was maintained in the range of 90 ℃ for 30 min. Immediately, 200 mL of warm distilled water (40℃) was added to the mixture, and it was treated with 18 mL of H_2O_2 (30%). Finally, the mixture was washed in 200 mL of 10% HCl solution and deionized water to remove metal ions by filter paper. The GO powder was obtained after being dried at room temperature for 24 h [33].

500 mg of GO powder was dispersed in 100 mL of deionized water by sonication using an ultrasonic homogenizer at 50 Hz frequency for 60 min. 400 mL of aqueous extract was added to the obtained GO solution and stirred at 90 ˚C for 8 hours. The final product was separated by centrifugation, washed several times in deionized water, and dried. The pH of GO suspensions was adjusted to 3 and 10, and the synthesized products were labeled as RGO.3 (acidic, pH: 3) and RGO.10 (basic, pH: 10). The initial pH of the lemon extract was 2.5.

Preparation of Fe_3O_4/RGO nanocomposite

In the first step, 0.5 g RGO.3 was dispersed in 10 ml of water for 15 min under magnetic stirring. In the second step, 100 mL of iron chloride hexahydrate salt with a concentration of 0.7 M and 10 mL of the lemon extract were added to the above-prepared solution. The prepared NaOH solution with a concentration of 2 M was then added dropwise to the mentioned mixture under stirring at 25 ˚C until the pH reached 10. In this step, the mixture was passed through the filter paper, washed in distilled water, and dried for 24 h. The Fe_3O_4/RGO powder was placed in a microwave oven at an output power of 500 W for 30 min.

Instruments and Characterisation

An ultrasonic homogenizer model 400ut (Fanavari Iranian Pajouhesh Nasir, Iran) was used to prepare the RGO solution, operated at a frequency of 50 Hz and power of 100 W. The pH of the solutions at all steps was measured with a pH meter (Metrohm-827, USA). A centrifuge Model 5430R (Eppendorf, Germany) was used to separate the phases. A programmed controller was used to dry all samples (JEIO TECH-CF- 02G, Korea). The concentration of Pb ions was measured using an atomic absorption spectrophotometer (Shimadzu, AA-680, Japan). The structure of all samples was observed using an FE-scanning electron microscope (Hitachi S4160, Japan). The XRD patterns of GO and RGOs were recorded on a diffractometer from Philips Company with Cu–K_α radiation. Raman spectroscopies were registered by an Apus+ Raman Microscope (Teksan, Iran) equipped with a 532 nm laser excitation at room temperature. The FTIR spectra were registered by an FTIR WQF-510 (Rayleigh, China) spectrometer by dispersing the samples in KBr pellets. BET surface area was investigated by N_2 ads/des isothermal liquid nitrogen temperature using a BELSORP-max.

Batch adsorption experiments

The effect of four parameters (solution pH, Fe_3O_4/RGO dosage, contact time, and initial concentration of Pb (II) ions) on batch adsorption was investigated. The experiments on solution pH were performed in a pH range of 1-8, with a lead concentration of 100 mg/L and 0.01 g of Fe_3O_4/RGO nanocomposite. The experiments of Fe_3O_4/RGO dosage were performed in a range of 0.01-0.07 g, with a lead concentration of 100 mg/L, and a pH of 5.0. The kinetic studies were performed at different times (1-60 min) by adding 0.05 g of Fe_3O_4/RGO to 30 mL of lead solution in concentrations of 100 mg/L. Equilibrium studies were performed at different concentrations (25-200 mg/L) by adding .05 g of Fe_3O_4/RGO to 30 mL of lead solution. All adsorption experiments were carried out in 250 mL Erlenmeyer flasks at room temperature.

The amount of Pb (II) ions adsorbed per unit mass of Fe_3O_4/RGO was determined using the following equation:

$$q_e = \frac{(C_o - C_e)V}{m} \quad (1)$$

The percentage of Pb (II) ion removal was determined using the following equation:

$$\%\,\mathrm{Re}moval = \frac{(C_o - C_e)}{C_o} \times 100 \quad (2)$$

where C: the concentrations of lead solution (mg/L), the subscripts "o" and "e" refer to initial and equilibrium values, q: equilibrium adsorption capacity (mg/g), V: the volume of lead solution (L), and m: the amount of Fe_3O_4/RGO used (g).

Kinetics and diffusion studies

In this section, the adsorption rate of lead ions onto Fe_3O_4/RGO adsorbent is evaluated using three models: pseudo-first-order (PFO), pseudo-second-order (PSO), and intra-particle diffusion models (IPD).

Based on Lagergren or PFO model, the adsorption rate is proportional to saturation concentration and the amount of adsorbate uptake [12]. This linear model is expressed by the following equation:

$$\log(q_e - q_t) = \log\ q_e - \frac{k_1}{2.303}t \quad (5)$$

where q_t and q_e are the amounts of Pb (II) adsorbed on the adsorbent at time t and equilibrium (mg/g), and k_1 is the rate constant of PFO model (1/min). The values of Lagergren constants can be obtained by plotting log (q_e–q_t) versus t.

The PSO model evaluated the amount of adsorbate uptake on the adsorbent [6]. The linear equation is expressed by the following equation:

$$\frac{t}{q_t} = \frac{1}{k_2 q_e^2} + \frac{1}{q_e}t \quad (6)$$

where q_t and q_e = the amounts of Pb (II) adsorbed on the adsorbent at time t and equilibrium (mg/g), and k_2 = the rate constant of the PSO model (g/mg min). The values of PSO constants can be defined by plotting t/q_t versus t.

The diffusion of adsorbate from the solution inside the adsorbent particle has several steps, including the creation of a film layer surrounding the adsorbent surface, then migration from this film into the adsorbent pores, and finally, the interaction between the adsorbate and adsorbent such as chemisorption, physisorption, ion exchange, or complexation. One of these steps has the slowest rate that controls the rate of the adsorption process [34]. The IPD model is expressed by the following equation:

$$q_t = k_i t^{0.5} + y \quad (7)$$

where q_t = the amounts of Pb (II) adsorbed on the adsorbent at time t (mg/g), k_i = the rate constant of IPD (mg/g min $^{0.5}$), and y is the intercept.

Isotherm studies

In this section, the experimental data of lead adsorbed on Fe_3O_4/RGO adsorbent is evaluated using three models: Langmuir, Freundlich, and Dubinin-Radushkevich isotherm.

Based on the Langmuir isotherm, the adsorption process is a monolayer and homogeneous process [35]. The linear model is defined by the following equation:

$$\frac{C_e}{q_e} = \frac{1}{q_{\max} k_L} + \frac{C_e}{q_{\max}} \quad (8)$$

where q_{max} and k_L = the maximum amount of lead adsorbed at equilibrium (mg/g) and the Langmuir constant related to the energy of adsorption (L/mg). The values of this model can be defined by a linear plot of C_e/q_e versus C_e.

The dimensional factor or R_L is used to investigate the feasibility of the Langmuir isotherm [36] and the kind of adsorption that is favorable if $0 < R_L < 1$. This factor is defined by the following equation:

$$R_L = \frac{1}{1 + k_L C_o} \quad (9)$$

The Freundlich isotherm is presented as a multilayer and heterogeneous process [6] and its linear model is defined by the following equation:

$$\log q_e = \log k_F + \frac{1}{n}\log C_e \quad (10)$$

In this formula, k_F: Freundlich constant (mg/g) and n: Freundlich exponent related to the adsorption intensity (dimensionless). The values of this model can be defined by a linear plot of log q_e

versus log C_e.

The Dubinin–Radushkevich (D-R) isotherm can be applied to investigate the nature of adsorption. The linear model of the (D-R) isotherm is defined by the following equation:

$$\ln q_e = \ln q_m - k_D \varepsilon^2 \quad (11)$$

where q_m = the theoretical adsorption capacity (mmol/g), k_D = the constant related to the medium energy of adsorption (mol^2/kJ^2), and ε = the Polanyi potential, which can be calculated from the following equation:

$$\varepsilon = RT \ln\left(1 + \frac{1}{C_e}\right) \quad (12)$$

where R (8.314 J/mol.K) and T (K) is the ideal gas constant and absolute temperature, respectively. The calculated value of K_D related to the adsorption energy, E, is defined by the following equation:

$$E = \frac{1}{\sqrt{2k_D}} \quad (13)$$

The kind of adsorption can be investigated by E values [37]:

E < 8 kJ/mol physical adsorption

8 < E kJ/mol chemical adsorption

Error analysis

To determine the conformity between kinetic equations and the experimental data, chi-square (X^2) and average relative error (ARE) were calculated [36]. These non-parametric equations are defined as:

$$X^2 = \sum_{i=1}^{N} \frac{(q_{e,\exp} - q_{e,cal})^2}{q_{e,\exp}} \quad (3)$$

$$ARE = \frac{100}{N} \sum_{i=1}^{N} \left| \frac{q_{e,\exp} - q_{e,cal}}{q_{e,\exp}} \right|_i \quad (4)$$

where $q_{e,exp,}$ and $q_{e,cal}$ refer to experimental and calculated equilibrium adsorption capacities and N refers to the number of observations in the experimental data.

RESULTS AND DISCUSSION

Characterization of RGOs

Sharp diffraction peaks were observed at 10.8° with an interlayer distance of 0.81 nm for the GO, and this peak was assigned as crystal planes (001) (Fig. 1). According to Fig. 1, the X-ray diffraction patterns of synthesized RGOs from GO using lemon extract exhibited a broad diffraction peak at 2θ of 23.8 and 23.2 (002 crystal plane) at initial pH of 3 and 10, respectively, indicating the successful reduction of GO. The calculated interface spacing ($d_{spacing}$) is 0.37 and 0.38 nm for RGO.3 and RGO.10, respectively, indicating a decrease in $d_{spacing}$ of RGOs with a decrease in the pH values and the synthesized RGOs had smaller $d_{spacing}$ than the GO because the oxygen-containing groups were partially removed. It proves the presence of RGOs with well-ordered 2D sheets and the lower population of oxygen-containing functional groups in RGO.3 than RGO.10 [38]. The main peck for RGO.3 is a sharpener in comparison to RGO.10, indicating that reduction in acidic condition leads to few-layer sheets with more crystallinity.

Raman spectrum was an important technique to analyze the defects and disorders associated with GO. Two significant peaks of the D-band - and G-band have been studied; structural edge defects (sp^3-hybridized) and E_{2g} vibration mode of planar sp^2 carbon (sp^2-hybridized), respectively [39]. According to Fig. 2, the D-band of GO, RGO.3, and RGO.10 were seen at 1363, 1379, and 1368 cm^{-1}, whereas the corresponding G-band was seen at 1609, 1573, and 1583 cm^{-1}, respectively. The ratio between the D-band and G-band intensity of (I_D/I_G) is related to the defect level, the sp^3/sp^2 carbon ratio, and the number of functional groups [40]. Obtained results showed that the I_D/I_G of GO (0.90) is lower than the value of RGO.3 (0.96) and RGO.10 (0.92), implying an increase in the number of sp^3 bonds and a decrease in the average size of the sp^2 domain. The increase is due to the GO reduction and the removal of oxygen functional groups using lemon extract. This ratio has increased for RGO.3 in comparison with RGO.10, indicating repairing defects in RGO sheets at pH 3.

The chemical structures of the RGO.3 and

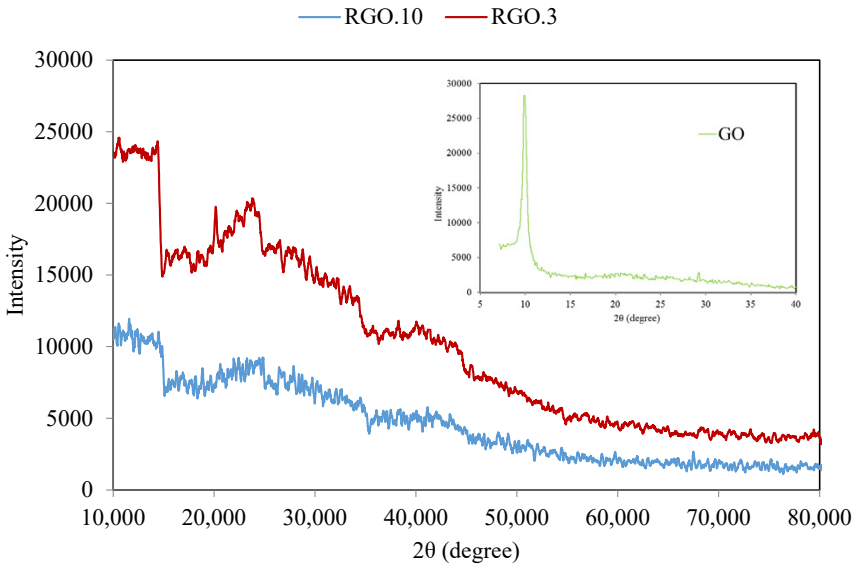

Fig. 1. The XRD patterns of GO, RGO.3, and RGO.10

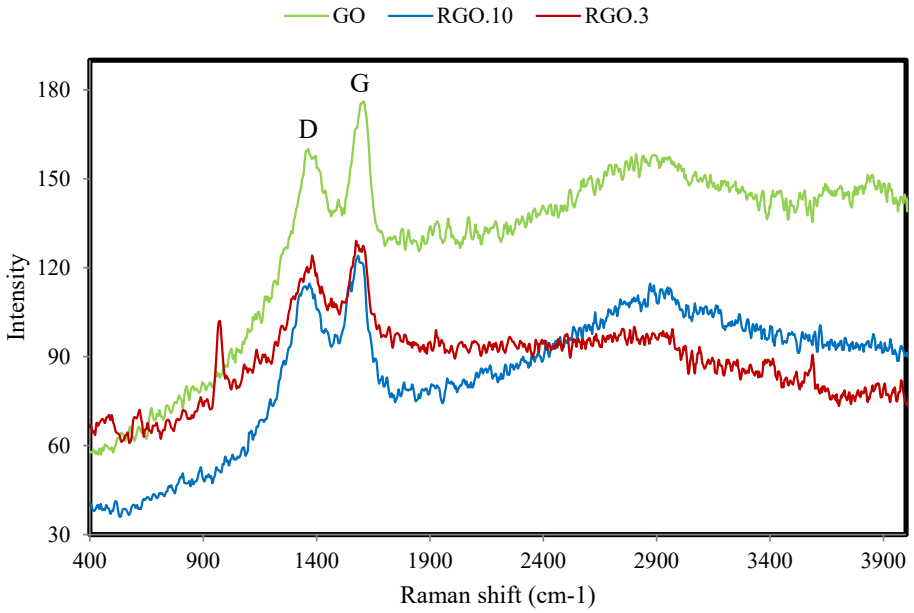

Fig. 2. Raman spectra of GO, RGO.3 and RGO.10

RGO.10 samples were studied by FTIR spectroscopy and are illustrated in Fig. 3. According to Fig. 3, Four important bands appeared in the GO spectrum, including C–O (1060 cm^{-1}), C–OH (1226 cm^{-1}), O–H (1412 cm^{-1}), and C = O (1733 cm^{-1}) [41], while these peaks did not appear in the synthesized RGOs spectrum or peaks intensity are low due to removal of the oxygen-containing groups. After reducing GO with lemon extract, two bands appear around 1580 and 1630 cm^{-1}, attributed to the aromatic υ (C=O) stretching, and another band at 1114 and 1110 cm^{-1} corresponding to the in-plane δ (C=C), which evidences the restoration of sp^2 structure in RGO.10, and RGO.3, respectively [31]. The increasing intensity of the above-mentioned absorption peaks was observed with the increase of the pH values from 3 to 10. The obtained FTIR spectra of the RGOs with lemon extract were

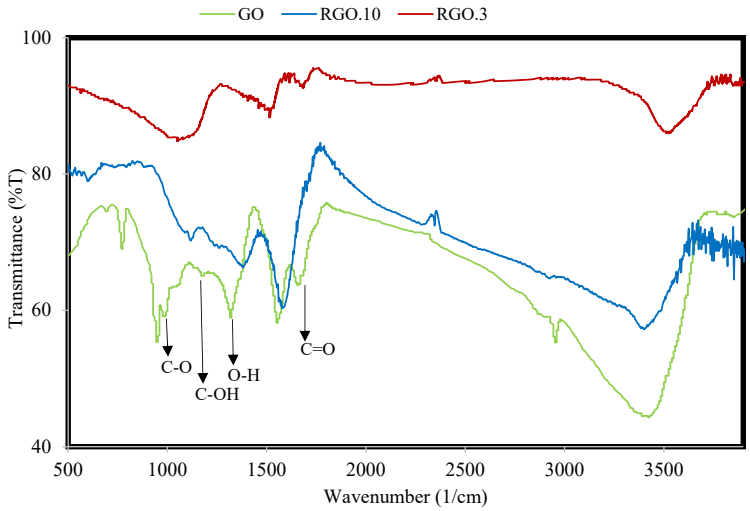

Fig. 3. The FT-IR spectra of GO, RGO.3, and RGO.10

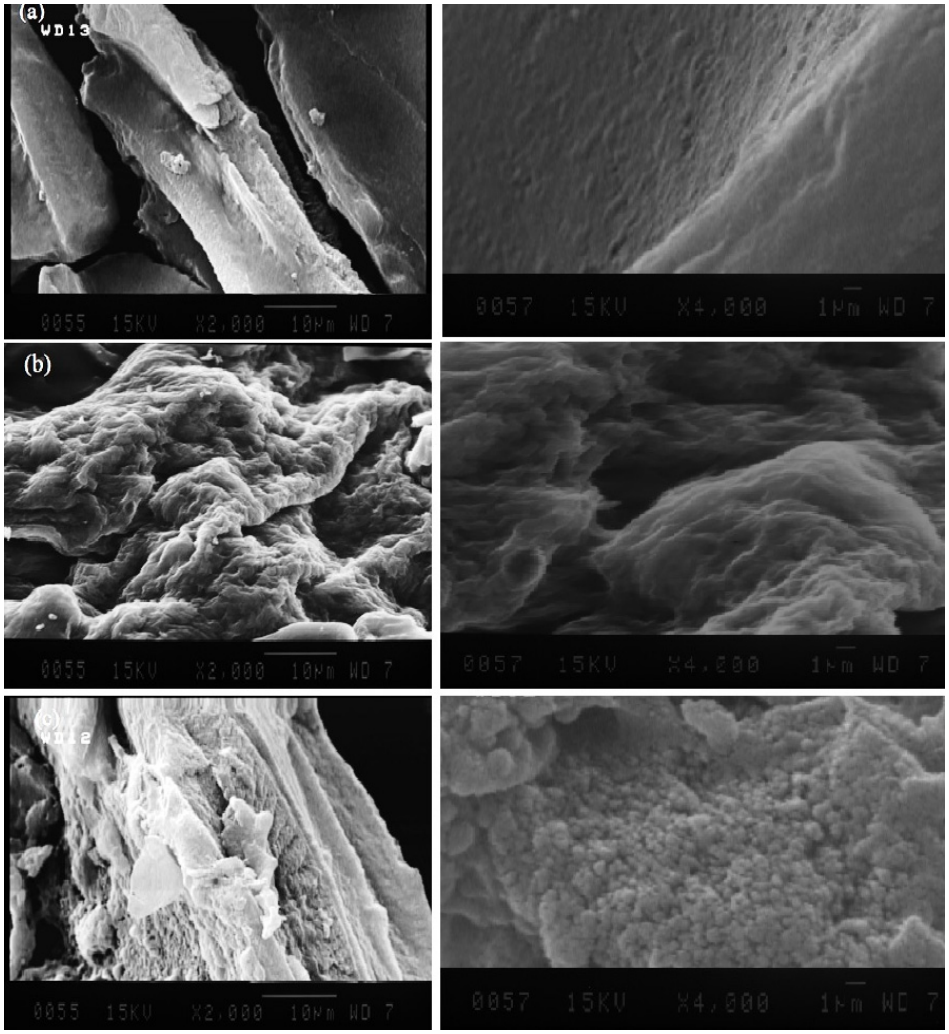

Fig. 4. SEM images of (a) GO, (b) RGO.3, and (c) RGO.10 with different magnifications (Scale bar 10 and 1 µm).

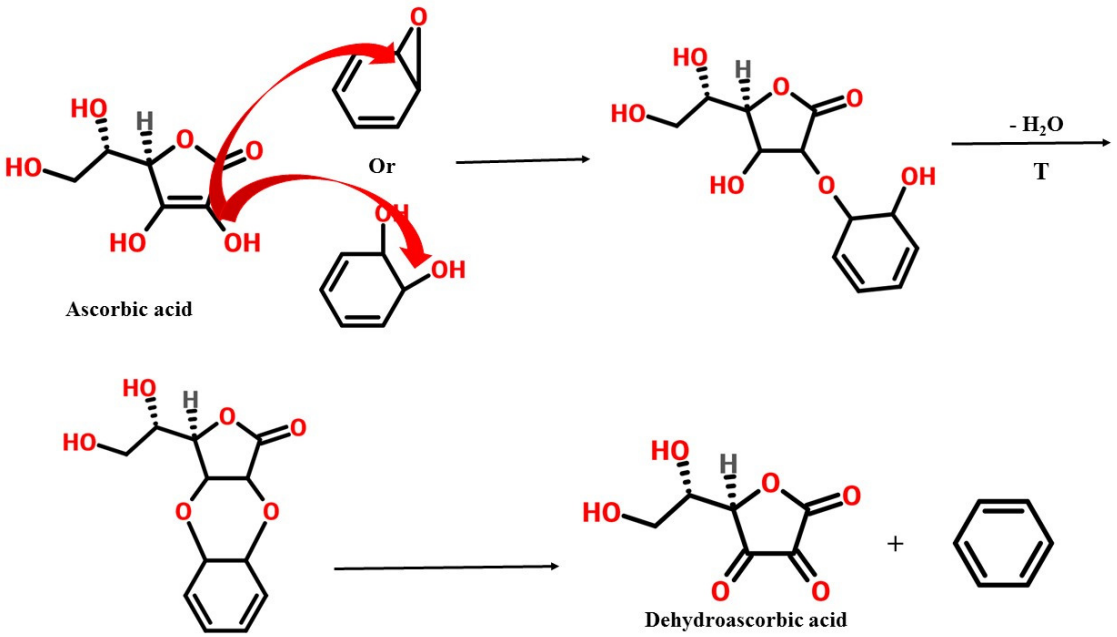

Fig. 5. Proposed mechanisms for the reduction of epoxide and hydroxyl groups with ascorbic acid

almost identical to that of the hydrazine-reduced RGO reported earlier [42].

The FESEM images of GO and RGOs were obtained and shown in Fig. 4 with different magnification. Fig. 4(a) shows oxidation sheets with the rough surface of GO, which was synthesized using the improved Hummer method. Fig. 4(b) indicates that RGO.3 forms dense agglomerates with a layered structure, and the nanosheets exhibit curved/wrinkled morphology that may be due to self-assembly via Vander Waals' force [43]. Uniform nanoporous structures and particle-like nanostructures were produced at a pH value of 10 (Fig. 4(c)).

Various natural reagents were utilized for the GO reduction such as Platanus orientalis [44], carrot root [45], Artemisia vulgaris [46], green tea extract [47], Punica Granatum peel extract [48], and Thymbra spicata extract [49]. The plant extracts were rich in phenolics, amino acids, caffeine, enzymes, vitamins, and proteins that have both reducing and stabilizing properties during the reduction process. They consist of oxygen, nitrogen, or sulfur functional groups which are able to reduce GO to RGO Similarly to the use of hydrazine as a GO reducing agent [50]. The typical I_D/I_G value for GO and RGO in reduction of the mentioned plant extracts is 0.8–1.29 and 0.79–1.30 respectively, which results in the decreasing of an average size of sp2 domains by reduction of GO [51].

Mechanism of GO reduction by lemon extract

In the lemon extract, there are chemical compounds such as alkaloids, vitamin C, acyclic and cyclic hydrocarbons, phenolic, and polyphenolic [52]. These compounds possess reducing and stabilizing properties. Vitamin C, known as ascorbic acid, is one of the important components present in the lemon extract, which is able to reduce GO sheets. The acidity of hydroxyl groups increases by releasing two protons of the ascorbic acid molecule and forming dehydroascorbic acid. The reduction process involves nucleophilic attack of oxygen anion of ascorbic acid to the epoxy or hydroxyl groups through a five-membered ring along with the release of a water molecule, as shown in Fig. 5. After that, the dehydroascorbic acid is broken down and can be converted to oxalic and guluronic acids (Fig. 6 (a)), and they could get adsorbed with the residual oxygen-containing groups of the RGO sheet via hydrogen bonds and stabilizes the RGO surface in the aqueous solution and prevent agglomeration and π-π interaction of the graphene sheets Fig. 6 (b)) [29, 50]. The reduction of GO was achieved in both acidic and alkaline conditions due

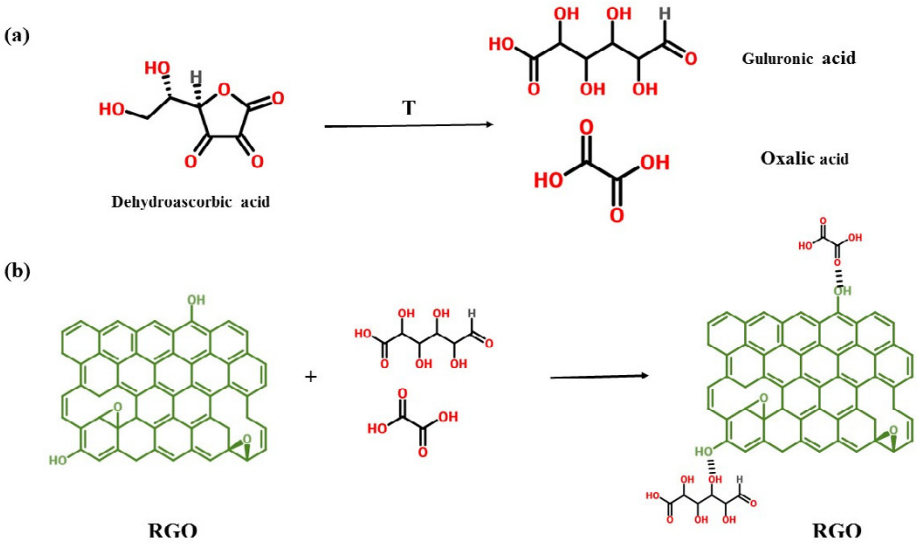

Fig. 6. Stabilization mechanism of the reduced GO aqueous suspension

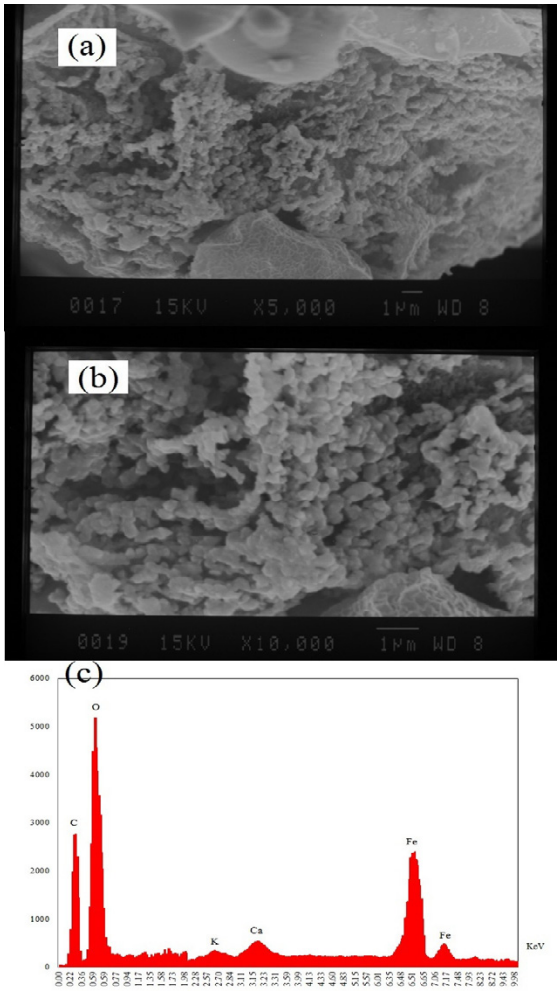

Fig. 7. SEM images of Fe_3O_4/RGO (a) ×5000, (b)×10000, and (c) EDS spectrum of Fe_3O_4/RGO

to the phytochemicals groups found in the lemon extract and these compounds converted to the benzoquinone form upon oxidation. The obtained results represented that the interaction between GO and the lemon extract at pH 3 leads to a more efficient reduction of GO in comparison to pH 10.

Characterization of Fe_3O_4/RGO

Fig. 7 presents the SEM images of the prepared Fe_3O_4/RGO nanocomposites at different magnifications. According to Fig. 7 (a) and (b), Fe_3O_4 nanoparticles are observed on RGO layers. These nanoparticles are spherical and uniformly distributed on the surface of RGO sheets. This phenomenon was confirmed by energy dispersive spectroscopy and is shown in Fig. 7 (c), where the Fe_3O_4/RGO nanocomposite mainly consists of C, O, and Fe elements. These results confirmed Fe_3O_4/RGO was successfully prepared.

Fig. 8 (a) shows the XRD pattern of Fe_3O_4/RGO nanocomposite. In synthesized nanocomposite, the presence of peaks at 2θ=24.1˚ and 2θ=26.6˚ indicates the characteristic reflection of reduced graphene oxide [19]. The peaks observed at 2θ=20.1˚, 30.07˚, 33.1˚, 35.7˚, 38.2˚, 40.8˚, 43.3˚, 49.4˚, 54.07˚, 55.4˚, 57.5˚, 62.3˚, and 63.9˚are related to Fe_3O_4 with a face-centered cubic structure [53]. The result confirmed that the nanocomposite was successfully synthesized. The sharp and strong peaks confirmed that the nanocomposite was well crystallized. The crystallite size of the Fe_3O_4 nanoparticles was determined as 23.78 nm using

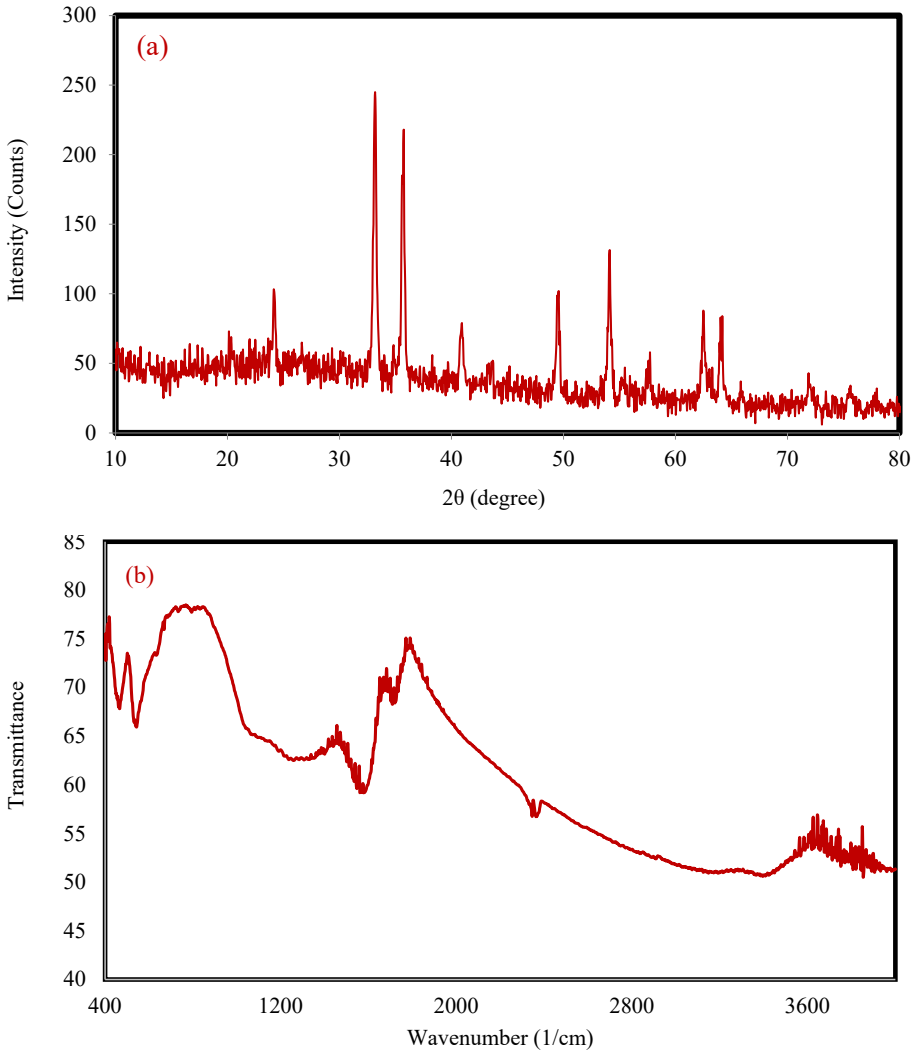

Fig. 8 (a) The XRD pattern, (b) FTIR spectrum, and (c) N2 ads/des isotherm and BJH pore size distribution plot of Fe_3O_4/RGO

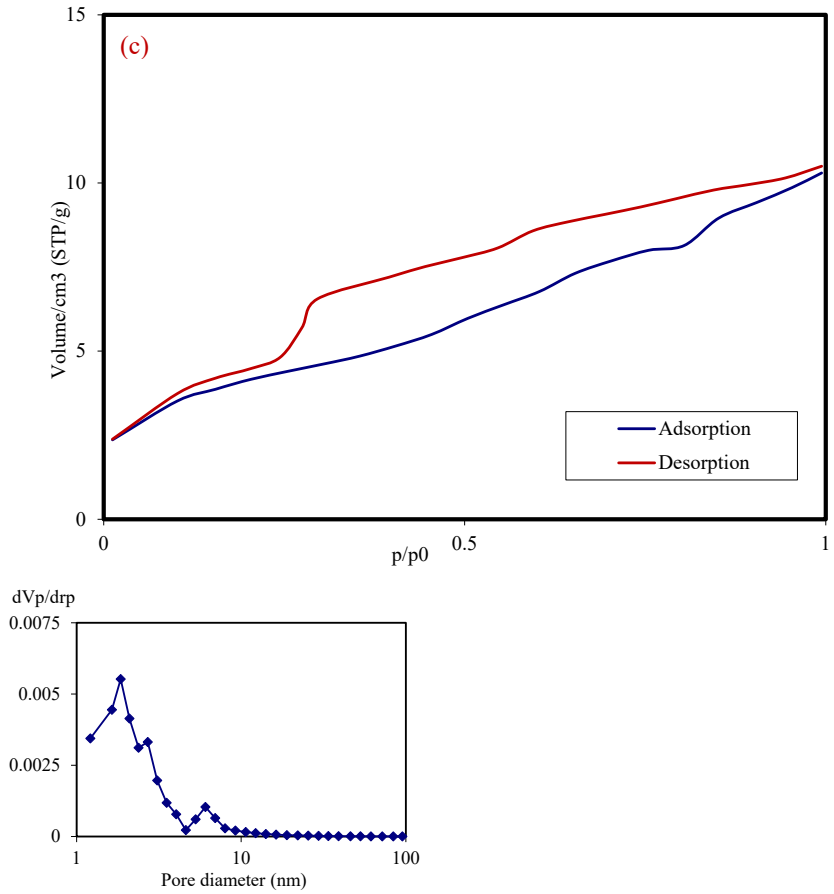

Continued Fig. 8 (a) The XRD pattern, (b) FTIR spectrum, and (c) N2 ads/des isotherm and BJH pore size distribution plot of Fe_3O_4/RGO

Debye–Scherrer's formula based on half the width of the (3 1 1) reflection.

The FTIR spectra of Fe_3O_4/RGO are shown in Fig. 8 (b). There were characteristic peaks at 400-600 cm^{-1} which relate to Fe-O stretching vibration [54]. The stretching vibrations of C=C and epoxy C-O-C at 1580 and 1255 cm^{-1} of RGO were present in the FTIR spectrum of the nanocomposite [55]. The peak at 3420 and 1720 cm^{-1} was assigned to OH/COOH on Fe_3O_4 particles and RGO sheets and C=O bonds. The above analysis indicates that the Fe_3O_4/RGO nanocomposite has been successfully prepared using lemon extract.

Fig. 8 (c) shows the ads/des curve of N_2 at 77 K and the differential pore size distribution estimated by the Barrett–Joyner–Halenda method. The N_2 adsorption/desorption curve indicates the type IV isotherm and confirms the presence of a mesoporous structure in the Fe_3O_4/RGO nanocomposite. BJH curve confirms the presence of the main mesoporous with diameters between 1 and 10 nm (average pore diameter, 4.43 nm). The specific surface area, total pore volume and, average pore diameter of Fe_3O_4/RGO sample were 14.29 m^2/g, 0.015 cm^3/g and, 4.43 nm, respectively.

Effect of different parameters on the removal of Pb ions

Effect of pH on removal

The initial pH of the ion solution can control the adsorption process, and this is due to the presence of hydrogen ions, positively charged metal ions in the bulk solution, and the competition between them. The surface charge and dissociation of functional groups on the adsorbent are affected by the pH of the solution. The type and behavior of the adsorbent with the type of adsorbed ion in the solution result in the effects of pH in the aqueous solution [56]. Fig. 9 (a) shows the effects of pH on the removal of Pb (II) ions on Fe_3O_4/RGO nanocomposite. It was noted that the adsorbed amounts for ions onto Fe_3O_4/RGO increased from 10.8 to 97.5% due to

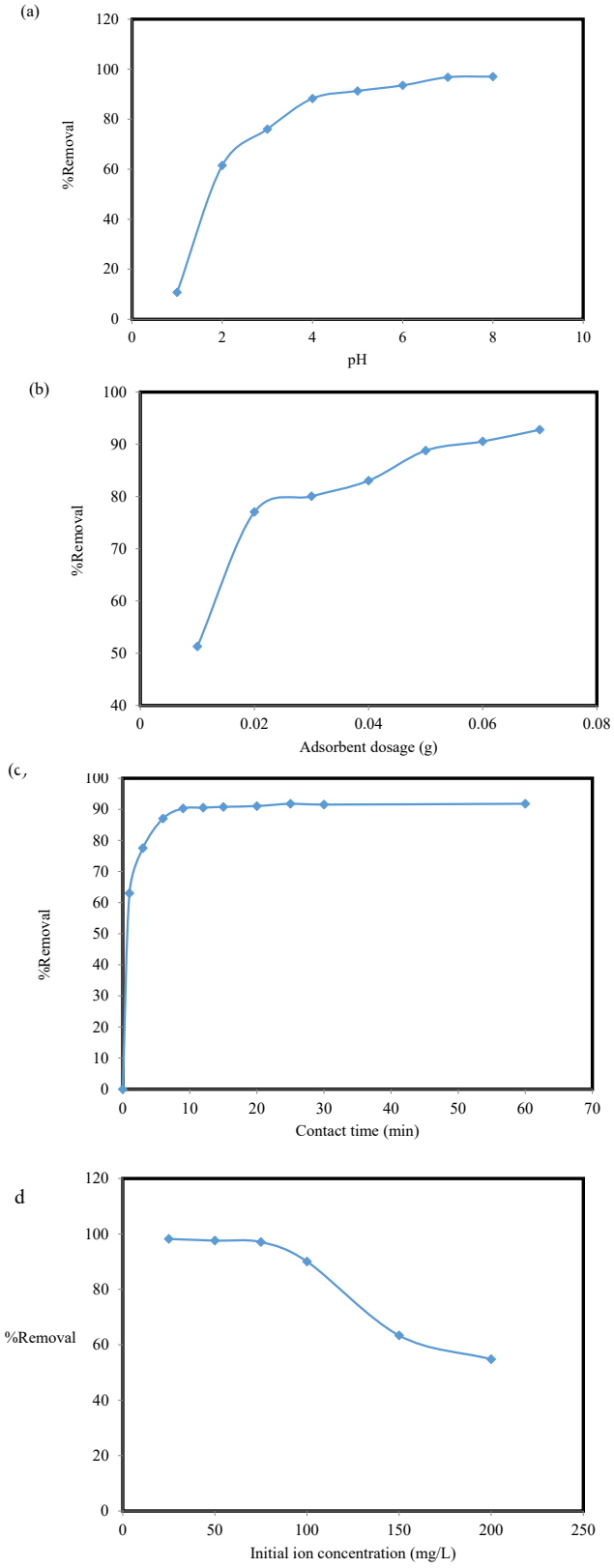

Fig. 9 (a) The effect of pH, (b) The effect of adsorbent dosage, (c) The effect of contact time, and (d) The effect of initial concentration on the sorption of Pb (II) onto Fe_3O_4/RGO nanocomposite.

the increase in pH from 1 to 8, and the Fe_3O_4/RGO adsorbent exhibited pH-dependent adsorption capacity on Pb ions. At pH 2–4, the percentage ion removal for nanocomposite adsorbent is very low due to the competition between additional hydrogen ions in the solution with Pb (II) for binding sites. Also, H^+ ions covered the surface of Fe_3O_4 nanoparticles and inhibited the adsorption of Pb ions. At pH 5–8, the carboxyl and hydroxyl groups of Fe_3O_4/RGO can be changed to $-COO^-$ and $-O^-$ groups, respectively, and might increase the electrostatic attraction between the adsorbent surface and Pb (II) ions [57]. In other words, the adsorption capacity of Fe_3O_4/RGO is in accordance with the surface oxygen contents. In this pH range of the solution, due to the deprotonation of the surface of Fe_3O_4 nanoparticles, Pb ions can adsorb on the surface of the adsorbent and result in an increase in percentage ion removal at higher pH in comparison to lower pH [58]. Also, the mechanism of lead adsorption on the RGO surface is cation–π interactions. Reduced GO has more sp^2 aromatic regions than GO, which leads to an increase in lead-π interaction. The optimized value of pH is 5.0 for the following experiments.

Effect of adsorbent dosage on removal

The effect of Fe_3O_4/RGO nanocomposite dosage on the percentage ion removal of lead ions is shown in Fig. 9 (b). It was shown that the ion removal of Pb (II) increased from 51.3 to 92.8% owing to the rise of the adsorbent dosage of Fe_3O_4/RGO from 0.01 to 0.07 g of the solutions. This increase in percentage lead ion removal is due to the increase in the number of active adsorption sites available for the adsorption of Pb (II) onto the surface of Fe_3O_4/RGO [59]. As can be seen in Fig. 9 (b), at higher concentrations of adsorbent, the ion removal of Pb (II) did not increase significantly with increasing Fe_3O_4/RGO. The optimized value of adsorbent dosage is 0.05 g for the following experiments.

Effect of contact time on removal

Fig. 9 (c) shows the effect of contact time between adsorbent and adsorbate on the percentage lead ion removal by Fe_3O_4/RGO nanocomposite from the model solution. The curve shows two stages; the first stage is rapid within the first 6 min, and about 87% of lead removal takes place in this stage. The second stage is slow, and the process reached equilibrium with 91.8% of lead removal. Rapid removal at the beginning of the process is due to the presence and availability of the vacant active sites of the Fe_3O_4/RGO adsorbent. Decreasing the vacant active sites of Fe_3O_4/RGO and creating electrostatic repulsion between the lead ions in both phases leads to a slow rate of adsorption at equilibrium conditions [60].

Effect of initial concentration on removal

The effect of initial lead concentration was measured, and the results are shown in Fig. 9 (d). It can be seen from this figure that the percentage of lead removal decreases from 98.2% to 54.7% on an increase in the concentration of lead ions from 25 to 200 mg/L. One of the most important factors for the removal of lead ions is the presence of active sites on the surface of the adsorbent, and there are more active and vacant sites at lower lead concentrations. By increasing the initial concentration and saturation of Fe_3O_4/RGO nanocomposite adsorbent

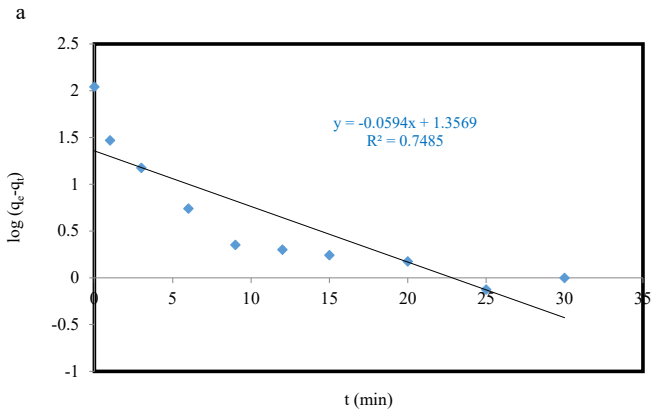

Fig. 10 (a) Linear pseudo-first-order kinetic plot, (b) linear pseudo-second-order kinetic plot and (c) intra-particle diffusion model plots.

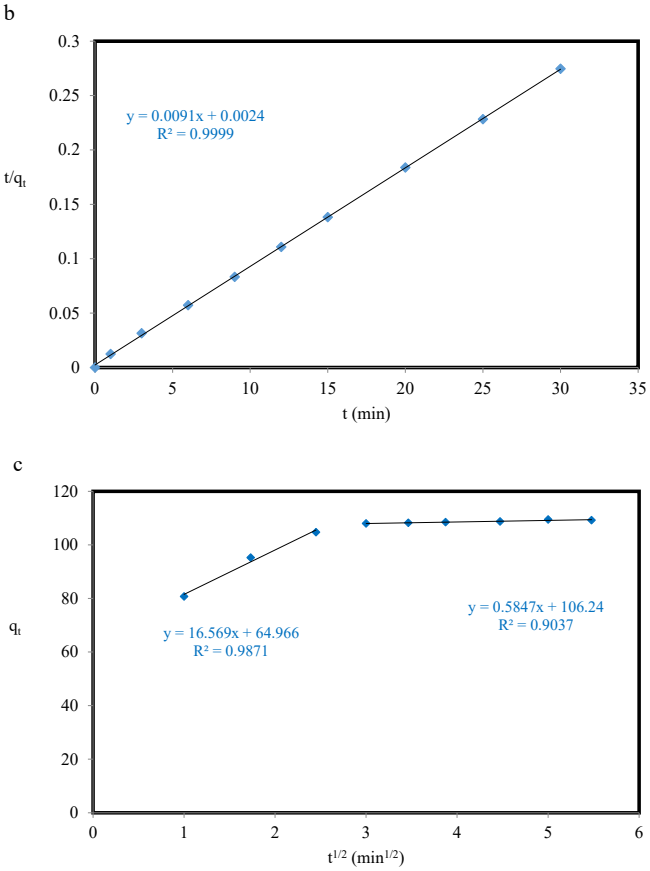

Continued Fig. 10 (a) Linear pseudo-first-order kinetic plot, (b) linear pseudo-second-order kinetic plot and (c) intra-particle diffusion model plots.

sites, the vacant sites decrease, which leads to a lower removal percentage [3].

Kinetics and diffusion studies

The obtained results of the kinetic models (Fig 10 (a-c)) are presented in Table 1. The data show that the adsorption of Pb (II) ions onto Fe_3O_4/RGO nanocomposite follows the PSO model with a higher R^2 value and lower ARE and X^2 values than PFO. Furthermore, the $q_{e,cal}$ value was very close to the $q_{e,exp}$ value, which confirms the high correlation between calculated and experimental data. According to these results, lead ions and Fe_3O_4/RGO adsorbent affect the adsorption process under optimum conditions, so the adsorption process of lead ions is a chemisorption process relating to the electrons exchanging or sharing [61]. The plot of q_t versus $t^{0.5}$ (Fig. (10)) does not pass through the origin and includes two regions, so two or three of the mentioned steps are involved in the adsorption of lead ions onto the adsorbent, and IPD is not the only rate-limiting step.

Isotherm studies

The influence of lead ion concentration on metal uptake capacity is shown in Fig. 11(a). The linear isotherm models and their obtained parameters are shown in Fig. 11 (b-d) and Table 2. By comparing the obtained R^2 values, it was found that the Langmuir isotherm ($R^2 > 0.99$) fitted better than other models that implied the monolayer coverage and homogenous distribution of lead ion adsorption onto the surface of the adsorbent. The maximum adsorption capacity (q_{max}) for Pb (II) ions onto Fe_3O_4/RGO nanocomposite was 107.52 mg/g. Also, the dimensional factor value was 0.030, which shows that the adsorption of lead ions on Fe_3O_4/RGO was favorable. According to Table 2, the R^2 value of the Freundlich isotherm is lower than that obtained using the Langmuir isotherm. Based on the D-R isotherm, the obtained value of E is greater than 8 kJ/mol, which implies that the

Table 1. Kinetic parameters for Pb (II) adsorption onto Fe_3O_4/RGO.

Model	Parameter	Values
	$q_{e,exp}$ (mg/g)	110.250
Pseudo-first-order	q_e (mg/g)	22.745
	k_1 (min -1)	0.136
	R^2	0.748
	ARE	7.936
	X^2	0.005
Pseudo-second-order	q_e (mg/g)	109.890
	k_2 (g/mg.min)	0.034
	R^2	0.999
	ARE	0.032
	X^2	9.67E-8
Intra particle diffusion	$k_{i,1}$ (mg/g.min$^{0.5}$)	16.569
	y (mg/g)	64.966
	R^2	0.987
	$k_{i,2}$ (mg/g.min$^{0.5}$)	0.584
	y (mg/g)	106.24
	R^2	0.903

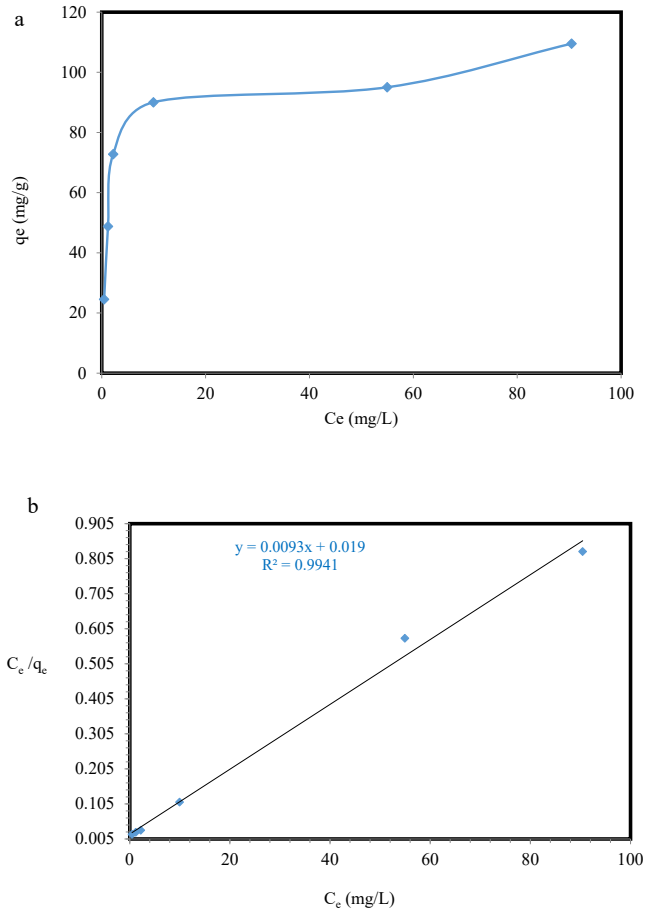

Fig. 11 (a) Effects of initial concentration for the removal of Pb (II) onto Fe^3O^4/RGO nanocomposite, (b) Langmuir isotherm plot, (c) Freundlich isotherm plot, and (d) Dubinin-Radushkevich isotherm plot.

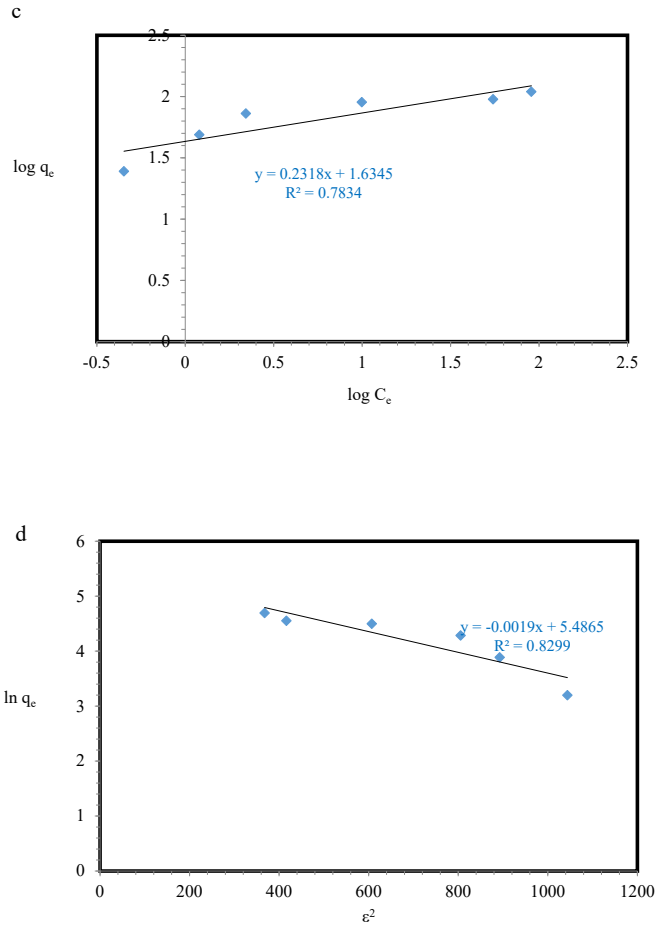

Continued Fig. 11 (a) Effects of initial concentration for the removal of Pb (II) onto Fe^3O^4/RGO nanocomposite, (b) Langmuir isotherm plot, (c) Freundlich isotherm plot, and (d) Dubinin-Radushkevich isotherm plot.

Table 2. Isotherm parameters obtained for Pb (II) adsorption onto Fe_3O_4/RGO.

Model	Parameter	values
Langmuir	k_L (L/mg)	0.489
	q_{max} (mg/g)	107.526
	R_L	0.030
	R^2	0.994
Freundlich	k_F (mg/g)	43.102
	n	4.314
	R^2	0.783
Dubinin–Radushkevich	k_D (mol^2/kJ^2)	0.0019
	q_m (mmol/g)	1.165
	E (kJ/mol)	22.360
	R^2	0.829

Table 3. Comparison of the maximum adsorption capacities of Pb (II) ions onto various adsorbents.

Adsorbent	Pb (II) concentration (mg/L)	q_{max} (mg/g)	References
1,5-diaminonaphthalene RGO	100	0.056	[18]
RGO	2-50	6.94	[43]
Reduced sulphonated graphene oxide	1-30	415	[44]
magnetic chitosan-functionalised 3D graphene	10-50	957.28	[45]
rGO/Fe3O4@PDA	n.a	42.73	[46]
GO	1-50	555	[47]
Fe_3O_4/RGO	25-200	107.526	This study

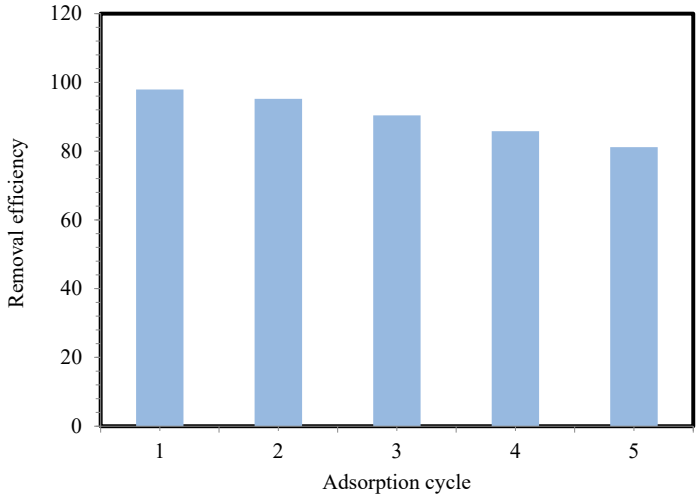

Fig. 12. Reuse experiment for Fe_3O_4/RGO adsorption of Pb(II)

adsorption process of lead ions onto Fe_3O_4/RGO nanocomposite was chemical sorption.

During the reduction process, the oxygen-containing groups were decreased on the surface of GO leading to increased Lewis alkalinity and the electrostatic attraction of RGO. This property increases the adsorption performance of Pb(II) [62]. Moreover, the reactions between Pb ions and electrons on the π-bond on the surface of RGO and the electrostatic attraction between Pb ions and Fe_3O_4 nanoparticles lead to the removal of Pb ions by Fe_3O_4/RGO nanocomposite [53].

The results of Pb (II) ion removal in this research were compared with other literature and listed in Table 3 [18, 62-66]. The difference in the q_{max} values of the various functionalized RGO is related to the difference in the kind of functionalized agent, reducing agent, different experimental conditions, etc.

Recyclability and stability studies

Recycling experiments, as a significant factor for its practical application, were performed five times to check the reusability of Fe_3O_4/RGO nanocomposite. Firstly, a solution of HCl (0.1 M) was used to desorb Pb ions from the nanocomposite, and then the nanocomposite was washed with deionized water to reach neutral pH. After five cycles of adsorption-desorption, the removal efficiency of Pb ion is shown in Fig. 12. As can be seen in Fig. 12, Even after five adsorption-desorption regenerations, the Fe_3O_4/RGO (81.1%) of removal efficiency on Pb(II), indicates that the magnetic nanocomposite has great potential as a reusable sorbent.

CONCLUSIONS

In this study, we successfully synthesized RGO using lemon extract (as the green reducing agent) by reducing GO under acidic and alkaline conditions. The internal structure of the RGOs, studied with Raman spectroscopy and XRD patterns, confirms better repair of the sp^2 graphitic lattice and a larger lattice size with decreasing pH. Magnetic reduced

graphene oxide (Fe_3O_4/RGO) nanocomposite was synthesized using the microwave method and was used as an effective adsorbent for lead removal. The obtained results of XRD, FTIR, SEM, and BET analysis showed that Fe_3O_4 nanoparticles were spherical with a diameter of 1-10 nm and uniformly covered the surface of RGO. The high adsorption performance towards lead ions was mainly attributed to the π–π stacking and the electrostatic interactions between Pb (II) and the RGO layers. The adsorption kinetics and isotherm are better described by the pseudo-second-order (electrons exchanging or sharing) and Langmuir models (homogeneous adsorption). The maximum monolayer adsorption capacity of the Fe_3O_4/RGO was found to be 107.52 mg/g with the monolayer process. In addition, the Fe_3O_4/RGO maintained good adsorption performance after five adsorption-desorption cycles, the removal efficiency of Pb(II) reached 81.1%, indicating that the nanocomposite has reusable value.

ACKNOWLEDGMENTS

The authors would like to thank the Science and Technology Park of Hamadan for its support.

CONFLICTS OF INTEREST

There are no conflicts to declare.

REFERENCES

[1] Kumar R, Bhattacharya S, Sharma P, Novel insights into adsorption of heavy metal ions using magnetic graphene composites, Journal of Environmental Chemical Engineering, 2021;9: 106212.

[2] Zarenezhad M, Zarei M, Ebratkhahan M, Hosseinzadeh M, Synthesis and study of functionalized magnetic graphene oxide for Pb2+ removal from wastewater, Environmental Technology & Innovation. 2021;22: 101384.

[3] Ghasemi M, Naushad M, Ghasemi N, Khosravi-fard Y, Adsorption of Pb(II) from aqueous solution using new adsorbents prepared from agricultural waste: Adsorption isotherm and kinetic studies, J. Ind. Eng. Chem. 2014;20: 2193–2199.

[4] Tao Y, Zhang C, Lü T, Zhao H, Removal of Pb(II) Ions from Wastewater by Using Polyethyleneimine-Functionalized Fe^3O^4 Magnetic Nanoparticles, Appl. Sci. 2020;10: 948.

[5] Farghali MA, Abo-Aly MM, Salaheldin TA, Modified mesoporous zeolite-A/reduced graphene oxide nanocomposite for dual removal of methylene blue and Pb2+ ions from wastewater, Inorganic Chemistry Communications 2021;126: 108487.

[6] Ghasemi M, Naushad M, Ghasemi N, Khosravi-fard Y, A novel agricultural waste based adsorbent for the removal of Pb(II) from aqueous solution: Kinetics, equilibrium and thermodynamic studies, J. Ind. Eng. Chem. 2014;20: 454–461.

[7] Gupta VK, Pathania D, Agarwal S, Singh P, Adsorptional photocatalytic degradation of methylene blue onto pectin–CuS nanocomposite under solar light, J. Hazard. Mater. 2012;243: 179– 186.

[8] Gupta VK, Agarwal S, Pathania D, Kothiyal NC, Sharma G. Use of pectin–thorium (IV) tungstomolybdate nanocomposite for photocatalytic degradation of methylene blue, Carbohydr. Polym. 2013;96: 277– 283.

[9] Sharma G, Pathania D, Naushad Mu. Preparation, characterization and antimicrobial activity of biopolymer based nanocomposite ion exchanger pectin zirconium(IV) selenotungstophosphate: Application for removal of toxic metals, J. Ind. Eng. Chem. 2014;20: 4482–4490.

[10] Bushra R, Naushad Mu, Adnan R, ALOthman ZA, Rafatullah M. Polyaniline supported nanocomposite cation exchanger: Synthesis, characterization and applications for the efficient removal of Pb2+ ion from aqueous medium, J. Ind. Eng. Chem. 2015;21: 1112–1118.

[11] Kaur M, Kumari S, Sharma P, Removal of Pb (II) from aqueous solution using nanoadsorbent of Oryza sativa husk: Isotherm, kinetic and thermodynamic studies, Biotechnology Rep. 2020; 25: e00410.

[12] Ghasemi M, Javadian H, Ghasemi N, Agarwal S, Gupta VK. Microporous nanocrystalline NaA zeolite prepared by microwave assisted hydrothermal method and determination of kinetic, isotherm and thermodynamic parameters of the batch sorption of Ni (II), J. Mol. Liq. 2016;215: 161–169.

[13] Wang Z, Xu W, Jie F, Zhao Z, Zhou K, Liu H, The selective adsorption performance and mechanism of multiwall magnetic carbon nanotubes for heavy metals in wastewater, Sci Rep. 2020;11: 16878.

[14] Hanbali G, Jodeh S, Hamed O, Bol R, Khalaf B, Qdemat A, Samhan S, Dagdag O, Magnetic Multiwall Carbon Nanotube Decorated with Novel Functionalities: Synthesis and Application as Adsorbents for Lead Removal from Aqueous Medium, Processes. 2020;8: 986.

[15] Gupta VK, Suhas, Nayak A, Agarwal S, Chaudhary M, Tyagi I. Removal of Ni (II) ions from water using scrap tire, J. Mol. Liq. 2014;190: 215–222.

[16] Çiftçi TD, Coşkun Yİ, Removal of Pb(II) from Water Using (Fe_3O_4/Ni/Ni_xB) Magnetic Nanocomposites, Carob (Ceratonia siliqua) or Grape Seeds (Vitis vinifera). J. Water Chem. Technol. 2020;42: 185–195.

[17] Tao Y, Zhang C, Lü T, Zhao H, Removal of Pb(II) Ions fromWastewater by Using Polyethyleneimine-Functionalized Fe3O4 Magnetic Nanoparticles, Appl. Sci. 2020;10: 948.

[18] Olanipekun O, Oyefusi A, Neelgund GM, Oki A. Synthesis and characterization of reduced graphite oxide-polymer composites and their application in adsorption of lead, Spectrochim. Acta. A: Mol. Biomol. Spectrosc. 2015;149: 991-996.

[19] Kanishka K, Silva KD, Huang H-H, Yoshimura M. Progress of reduction of grapheme oxide by ascorbic acid, Appl. Surf. Sci. 2018;447: 338-346.

[20] Menazea AA, Ezzat HA, Omara W, Basyouni OH, Ibrahim SA, Mohamed AA, Tawfik W, Ibrahim MA, Chitosan/graphene oxide composite as an effective removal of Ni, Cu, As, Cd and Pb from wastewater, Computational and Theoretical Chemistry. 2020;1189: 112980.

[21] Weng X, Lin Z, Xiao X, Li C, Chen Z. One-step biosynthesis of hybrid reduced graphene oxide/iron-based nanoparticles by eucalyptus extract and its removal of dye, J. Clean. Prod.

2018;203: 22-29.
[22] Kadiyala NK, Mandal BK, Ranjan S, Dasgupta N. Bioinspired gold nanoparticles decorated reduced grapheme oxide nanocomposite using Syzygium cumini seed extract: Evaluation of its biological applications, Mater Sci Eng C Mater Biol Appl. Msc. 2018;93: 191-205.
[23] Dinari M, Haghighi A. Ultrasound-assisted synthesis of nanocomposites based on aromatic polyamide and modified ZnO nanoparticle for removal of toxic Cr(VI) from water. Ultrason. Sonochem. 2018;41: 75–84.
[24] Khatamian M, Khodakarampoor N, Saket Oskouia M, Kazemian N. Synthesis and characterization of RGO/zeolite composites for the removal of arsenic from contaminated water. RSC Adv. 2015;5: 35352-35360.
[25] Haq IU, Anwar AW, Waheed A, Arslan Z, Ilyas U, Munir A, A comparison of three-way synthesis and characterization of reduced graphene oxide–sulfur composite, Surface Review and Letters. 2012;28(10): 2150088.
[26] Ambrosi A, Chua C.K, Bonanni A, Pumera M. Lithium aluminum hydride as reducing agent for chemically reduced graphene oxides, Chem. Mater. 2012;24: 2292–2298.
[27] Wang G, Yang J, Park J, Gou X, Wang B, Liu H, Yao J. Facile synthesis and characterization of graphene nanosheets. J. Phys. Chem. C. 2008;112: 8192–8195.
[28] Ferna´ndez-Merino MJ, Guardia L, Paredes JI, Villar-Rodil S, Solı´s-Ferna´ndez P, Martı´nez-Alonso A, Tasco´n JMD. Vitamin C Is an Ideal Substitute for Hydrazine in the Reduction of Graphene Oxide Suspensions. J. Phys. Chem. C. 2010;114: 6426–6432.
[29] Zhang J, Yang H, Shen G, Cheng P, Zhang J, Guo S. Reduction of graphene oxide via L-ascorbic acid, Chem. Commun., 2010;46: 1112–1114.
[30] Martí N, Mena P, Cánovas JA, Micol V, Saur D. Vitamin C and the Role of Citrus Juices as Functional Food. Natural Product Communications. 2009;4(5): 677-700.
[31] Bosch-Navarro C, Coronado E, Marti-Gastaldo C, Sanchez-Royo JF, Gomez Gomez M. Influence of the pH on the synthesis of reduced graphene oxide under hydrothermal conditions. Nanoscale. 2012;4: 3977-3982.
[32] Bai Y, Rakhi RB, Chen W, Alshareef HN. Effect of pH-induced chemical modification of hydrothermally reduced graphene oxide on supercapacitor performance. Journal of Power Sources 2013;233: 313-319.
[33] Zahed M, Parsamehr Ps, Ahmadzadeh-Tofighy M, Mohammadi T. Synthesis and functionalization of graphene oxide (GO) for salty water desalination as adsorbent. Chem. Eng. Res. Des. 2018;138: 358-365.
[34] Ghasemi M, Mashhadi S, Azimi-Amin J. Fe^3O^4/AC nanocomposite as a novel nano adsorbent for effective removal of cationic dye: Process optimization based on Taguchi design method, kinetics, equilibrium and thermodynamics. J. Water Environ. Nanotechnol., 2018;3(4): 321-336.
[35] Agarwal S, Gupta VK, Ghasemi M, Azimi-Amin J. Peganum harmala-L Seeds adsorbent for the rapid removal of noxious brilliant green dyes from aqueous phase. J. Mol. Liq. 2017;231: 296–305.
[36] Asgari G, Roshani B, Ghanizadeh G. The investigation of kinetic and isotherm of fluoride adsorption onto functionalize pumice stone. J. Hazard. Mater. 2012;217–218: 123– 132.
[37] Güzel F, Sayğılı H, Sayğılı GA, Koyuncu F. New low-cost nanoporous carbonaceous adsorbent developed from carob (Ceratonia siliqua) processing industry waste for the adsorption of anionic textile dye: Characterization, equilibrium and kinetic modeling. J. Mol. Liq. 2015;206: 244–255.
[38] Narayanan KB, Kim HD, Han SS. Biocompatibility and hemocompatibility of hydrothermally derived reduced graphene oxide using soluble starch as a reducing agent. Colloids and Surfaces B: Biointerfaces. 2020;185: 110579.
[39] Nazarpour S, Hajian R, Hosseini-Sabzvari M. A Novel Nanocomposite Electrochemical Sensor based on Green Synthesis of Reduced Graphene Oxide/Gold Nanoparticles Modified Screen Printed Electrode for Determination of Tryptophan using Response Surface methodology Approach. Microchemical Journal. 2020;154: 104634,
[40] Mahmudzadeh M, Yari H, Ramezanzadeh B, Mahdavian M. Highly potent radical scavenging-anti-oxidant activity of biologically reduced graphene oxide using Nettle extract as a green bio-genic aminesbased reductants source instead of hazardous hydrazine hydrate. Journal of Hazardous Materials. 2019;371: 609–624.
[41] Mei X, Ouyang J. Ultrasonication-assisted ultrafast reduction of graphene oxide by zinc powder at room temperature, Carbon. 2011;49: 5389 –5397.
[42] Bahar S, Babamiri B. Determination of Zn(II) in rock and vegetable samples after acidic digestion followed by ultrasound-assisted solid-phase extraction with reduced graphene oxide as novel sorbent, in combination with flame atomic absorption spectrometry. J Iran Chem. Soc. 2014;11: 1039-1045.
[43] Weng X, Wu Jg, Ma L, Owens G, Chen Z. Impact of synthesis conditions on Pb(II) removal efficiency from aqueous solution by green tea extract reduced graphene oxide. Chemical Engineering Journal. 2019;359: 976-981.
[44] Xing FY, Guan LL, Li YL, Jia CJ, Biosynthesis of reduced graphene oxide nanosheets and their in vitro cytotoxicity against cardiac cell lines of Catla catla, Environ. Toxicol. Pharmacol. 2016;48: 110–115.
[45] Kuila T, Bose S, Khanra P, Mishra AK, Kim NH, Lee JH, A green approach for the reduction of graphene oxide by wild carrot root, Carbon. 2012;50: 914–921.
[46] Chettri P, Vendamani V,. Tripathi A, Pathak AP, Tiwari A, Self assembly of functionalised graphene nanostructures by one step reduction of graphene oxide using aqueous extract of Artemisia vulgaris, Appl. Surf. Sci. 2016;362: 221–229.
[47] Lin Z, Weng X, Ma L, Sarka B, Chen Zu, Mechanistic insights into Pb(II) removal from aqueous solution by green reduced graphene oxide, Journal of Colloid and Interface Science. 2019;550: 1–9
[48] Adyani SH, Soleimani E, Green synthesis of Ag/Fe^3O^4/RGO nanocomposites by Punica Granatum peel extract: Catalytic activity for reduction of organic pollutants, international journal of hydrogen energy. 2019;44: 2711-2730.
[49] Veisi H, Tamoradi T, Karmakar B, Mohammadi P, Hemmati S, In situ biogenic synthesis of Pd nanoparticles over reduced graphene oxide by using a plant extract (Thymbra spicata) and its catalytic evaluation towards cyanation of aryl halides, Materials Science & Engineering C. 2019;104: 109919.
[50] Navalóna S, Herance JR, Álvaro M, García H, General aspects in the use of graphenes in catalysis, Mater. Horiz. 2018;5: 363-378.
[51] Zheng Y, WangA, Cai W, Wang Z, Peng F, Liu Z, Fu L,

Hydrothermal preparation of reduced graphene oxide-silver nanocomposite using Plectranthus amboinicus leaf extract and its electrochemical performance, Enzyme and Microbial Technology. 2016;95: 112-117.
[52] AL-Jabri NN, Hossain MA. Chemical composition and antimicrobial potency of locally grown lemon essential oil against selected bacterial strain. Journal of King Saud University Science. 2018;30: 14–20.
[53] Xin X, Wei Q, Yang J, Yan L, Feng R, Chen G, Du B, Li H. Highly efficient removal of heavy metal ions by amine-functionalized mesoporous $Fe^{3}O^{4}$ nanoparticles. Chem. Eng. J. 2012;184: 132– 140.
[54] Bashiri F, Khezri M, Kalantary RR, Kakavandi B. Enhanced photocatalytic degradation of metronidazole by TiO_2 decorated on magnetic reduced graphene oxide: Characterization, optimization and reaction mechanism studies. Journal of Molecular Liquids. 2020;314: 113608.
[55] Hurtado RB, Cortez-Valadez M, Aragon-Guajardo JR, Cruz-Rivera JJ, Martınez-Sua rez F, Flores-Acosta M. One-step synthesis of reduced graphene oxide/gold nanoparticles under ambient conditions. Arabian Journal of Chemistry. 2020;13: 1633–1640.
[56] Ren Y, Yan N, Wen Q, Fan Z, Wei T, Zhang M, Ma J. Graphene/_-MnO_2 composite as adsorbent for the removal of nickel ions from wastewater. Chem. Eng. J. 2011;175: 1– 7.
[57] Cheng CS, Deng J, Lei B, He A, Zhang X, Ma L, Li S, Zhao C. Toward 3D graphene oxide gels based adsorbents for high-efficient water treatment via the promotion of biopolymers. J. Hazard. Mater. 2013;263: 467– 478.
[58] Srivastava V, Sharma YC, Sillanpää M. Application of response surface methodology for optimization of Co(II) removal from synthetic wastewater by adsorption on NiO nanoparticles. J. Mol. Liq. 2015;211: 613–620.
[59] Javadian H, Zamani-Sorkhrodi F, Koutenaei BB. Experimental investigation on enhancing aqueous cadmium removal via nanostructure composite of modified hexagonal type mesoporous silica with polyaniline/polypyrrole nanoparticles. J. Ind. Eng. Chem. 2014;20: 3678–3688.
[60] Mallakpour S, Behranvand V. Synthesis of mesoporous recycled poly(ethylene terephthalate)/MWNT/carbon quantum dot nanocomposite from sustainable materials using ultrasonic waves: Application for methylene blue removal. J. Clean. Prod. 2018;190: 525-537.
[61] Rahimi K. Mirzaei R, Akbari A, Mirghaffari N. Preparation of nanoparticle-modified polymeric adsorbent using wastage fuzzes of mechanized carpet and its application in dye removal from aqueous solution. J. Clean. Prod. 2018;178: 373-383.
[62] Lin Z, Weng X, Ma L, Sarkar B, Chen Z. Mechanistic insights into Pb(II) removal from aqueous solution by green reduced graphene oxide. J. Colloid. Interf. Sci. 2019;550: 1-9.
[63] Wei Mp, Chai H, Cao Yl, Jia Dz. Sulfonated Graphene Oxide as an Adsorbent for Removal of Pb2+ and Methylene blue. J. Colloid. Interf. Sci. 2018;524: 297-305.
[64] Nasiri R, Arsalani N, Panahian Y. One-pot synthesis of novel magnetic three-dimensional graphene/chitosan/nickel ferrite nanocomposite for lead ions removal from aqueous solution: RSM modelling design. J. Clean. Prod. 2018;201: 507-515.
[65] Mehdinia A, Heydari S, Jabbari A. Synthesis and characterization of reduced graphene oxide-Fe3O4@polydopamine and application for adsorption of lead ions: Isotherm and kinetic studies. Mater. Chem. Phys. 2020;239: 121964.
[66] Jun BM, Kima S, Kim Y, Her N, Heo J, Han J, Jang M, Park CM, Yoon Y. Comprehensive evaluation on removal of lead by graphene oxide and metal organic framework. Chemosphere. 2019;231: 82-92.